

Supporting Information

Amphiphilic confined Pt-based nanocatalysts produced by atomic layer deposition with enhanced catalytic performance for biphasic reactions

Shuangfeng Xing, Zhe Gao,* Shichao Zhao, Mi Xiong, Pengfei Wang, Jianyuan Zhang, Sen Wang, Guofu Wang, Yong Qin*

1. Experimental Section

Sample preparation.

Pretreatment of CNTs and the ALD process: Raw CNTs with specific diameters in the range of 60-100 nm (TCI Shanghai, >95%) were firstly pretreated with HNO₃ (68 wt.%) for 4 h at 110 °C to remove the existing metals and amorphous carbon, and then filtered and washed with deionized water until there was no further change in pH (around pH=7). After that, the obtained CNTs were dried at 100 °C for 12 h in an oven and then annealed at 900 °C for 2 h in Ar atmosphere.

The ALD process was carried out in a hot-wall, closed chamber-type ALD reactor. Prior to ALD, the pretreated CNTs (2 g) were dispersed in ethanol (100 mL) by ultrasonic agitation, and then 1 mL of the suspension was dropped onto a quartz wafer (10 cm×10 cm). After dried at ambient temperature, they were transferred to the ALD chamber. Pt nanoparticles were deposited at 250 °C with trimethyl (methylcyclopentadienyl) platinum (MeCpPtMe₃, Strem Chemicals, 99%) and ozone (O₃) as precursors. MeCpPtMe₃ was kept at 65 °C. The pulse, exposure, and purge times for the MeCpPtMe₃ were 0.5, 12, and 25 s, respectively, and for the O₃, 0.1, 12, and 25 s, respectively. The Al₂O₃ film was deposited at 125 °C with trimethylaluminum (TMA, Alfa Aesar, 25% in hexane) and deionized H₂O as precursors. The pulse, exposure, and purge times for the TMA were 0.02, 8, and 25 s, respectively, and for the H₂O, 0.1, 8, and 25 s, respectively. The TiO₂ film was deposited at 125 °C by using Titanium tetraisopropoxide (TTIP, Alfa Aesar, 97%) and deionized H₂O as precursors. The pulse, exposure, and purge times for TTIP were 1, 8, and 25 s, and those for H₂O were 0.1, 8, and 25 s, respectively. TTIP was maintained at 80 °C. The Polyimide (PI) film was deposited by sequentially exposing the samples to pyromellitic dianhydride (PMDA J&K 99.5%) and ethidene diamine (EDA) at 175 °C. PMDA and EDA were kept at 175 °C and 30 °C, respectively. The pulse, exposure, and purge times for PMDA were 5, 10, and 30 s and those for EDA were 0.1, 20, and 30 s, respectively.

Sample characterization.

A JEOL 2100F (FEI, Titan Cubed Themis G2 300), equipped with a Dual-Axis tomography holder, was used to acquire the TEM images and STEM tomography tilt series for 3D reconstruction. The tilt series were acquired over a tilt range of -50-50° with an image recorded every 1°. The XRD patterns were collected on a Bruker D8 Advance X-ray diffractometer using a Cu K α source ($\lambda=1.540 \text{ \AA}$) in the 2 θ range from 10° to 80°. Thermogravimetric (TG) analysis was performed with Setsys Evolution TGA 16/18 (SETARAM, France) in air at a heating rate of 10 °C min⁻¹ from ambient temperature up to 900 °C. The contents of Pt metal in the catalysts were determined by inductively coupled plasma atomic emission spectrometry (ICP-AES, Thermo iCAP 6300). Contact angle measurements were performed on an SL200KB (USA KINO) optical contact angle measuring apparatus at room temperature. The CNTs and TiO₂ nanotubes were squashed to a 3 mm-thick tablet. The carbon nanofilm sample were prepared by depositing 300 ALD cycles of PI on a silicon wafer and then annealed at 700 °C in a 5% H₂/Ar atmosphere. For the static water droplet contact angle measurement, a droplet of water was dropped on the surface of the sample. The photographs of water droplet were recorded by a CCD camera on the equipment. The air-bubble contact angles under water were measured by the captive bubble method.¹

2. Supplementary Figures and Tables

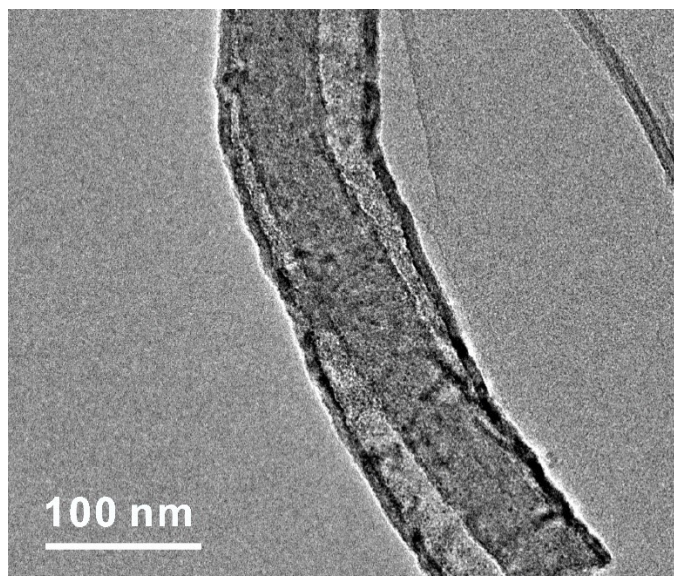


Figure S1. TEM image of $\text{TiO}_2/\text{Pt}@\text{CNT}$. In some rare cases, point of contact can be found in a certain position of the TEM image. Although there is a local point of contact, the tube-in-tube motif of the catalyst is still maintained, and the amphiphilic confined microenvironment also remains.

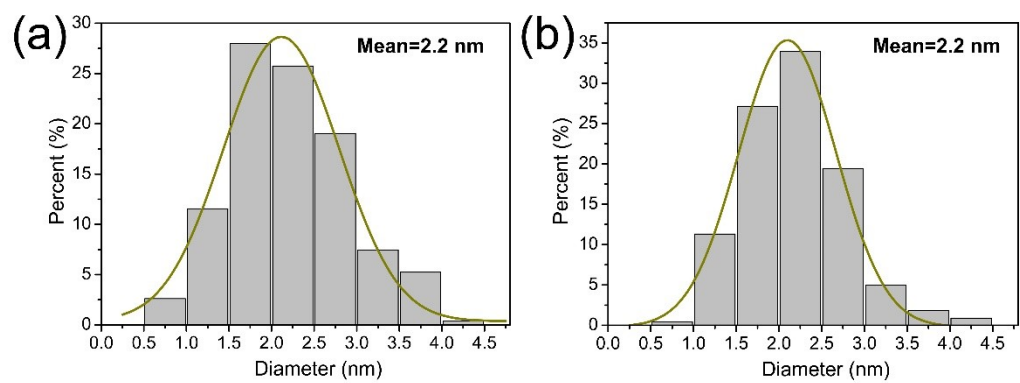


Figure S2. The particle size distributions of Pt nanoparticles in (a) TiO₂/Pt@CNT and (b) TiO₂/Pt@TiO₂/CNT.

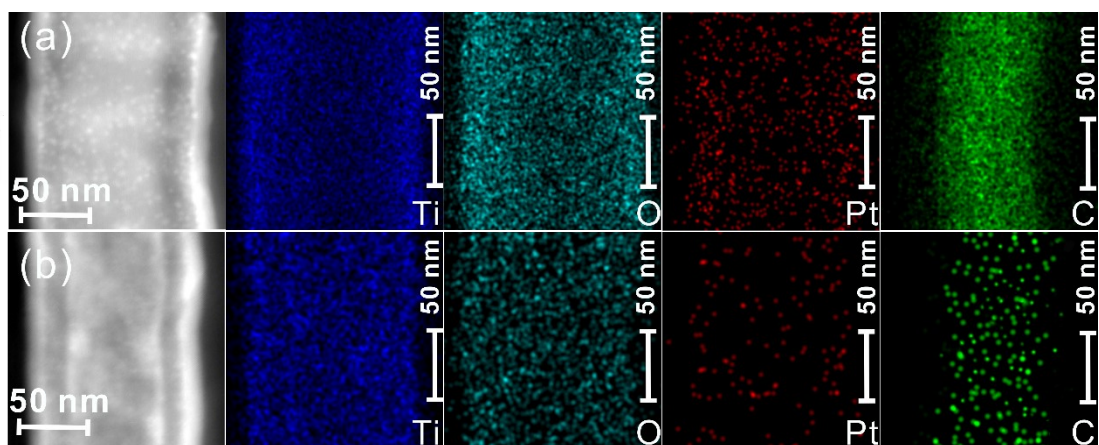


Figure S3. STEM images and the corresponding EDS mappings of (a) TiO₂/Pt@CNT and (b) TiO₂/Pt@TiO₂/CNT.

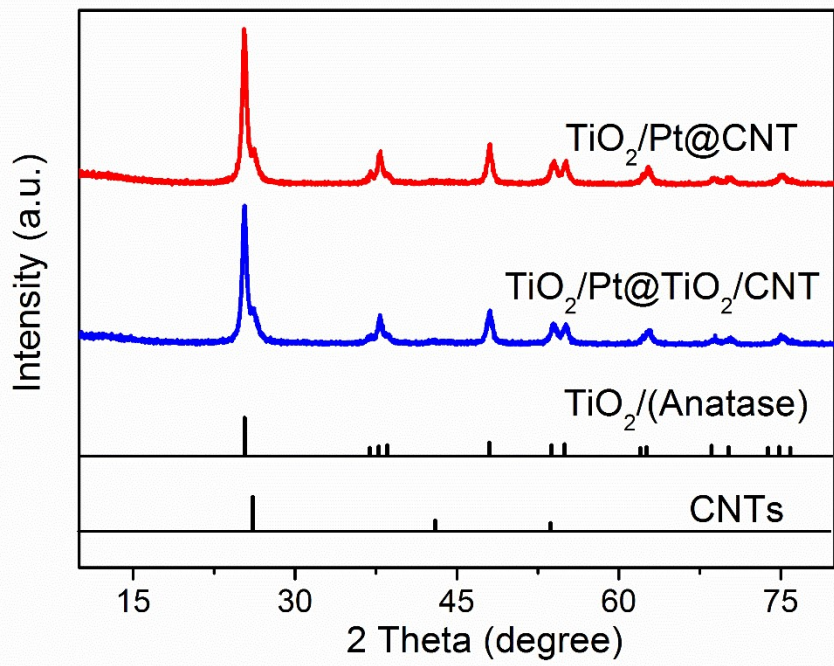


Figure S4. XRD profiles of $\text{TiO}_2/\text{Pt@CNT}$ and $\text{TiO}_2/\text{Pt@TiO}_2/\text{CNT}$.

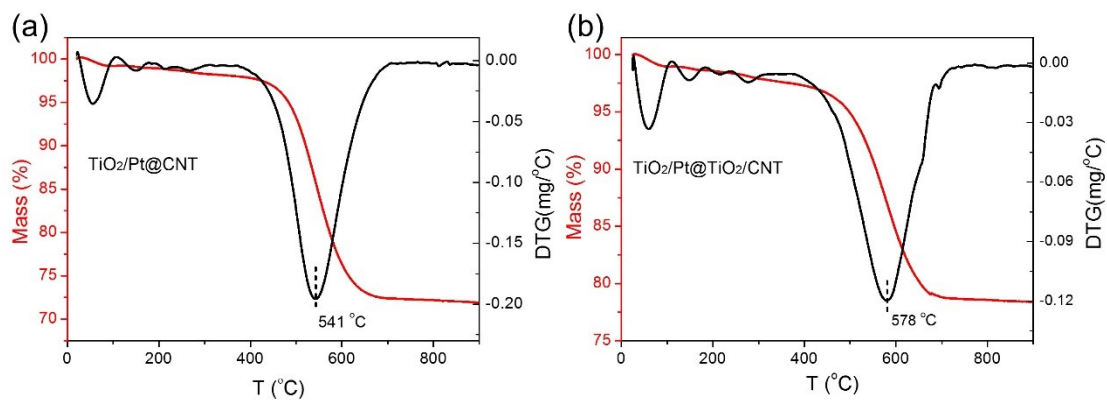


Figure S5. TG and DTG curves of (a) $\text{TiO}_2/\text{Pt}@/\text{CNT}$ and (b) $\text{TiO}_2/\text{Pt}@/\text{TiO}_2/\text{CNT}$. Both the samples exhibit a significant weight loss at 400-700 °C, due to the oxidation/combustion of CNTs. In the DTG curve of $\text{TiO}_2/\text{Pt}@/\text{CNT}$, the exothermic peak is centered at 541 °C. For $\text{TiO}_2/\text{Pt}@/\text{TiO}_2/\text{CNT}$, the peak shifts to a higher temperature (578 °C), which is due to the protection of the TiO_2 layer coating on CNTs. These results demonstrate that they maintain good thermal stabilities until 400 °C.

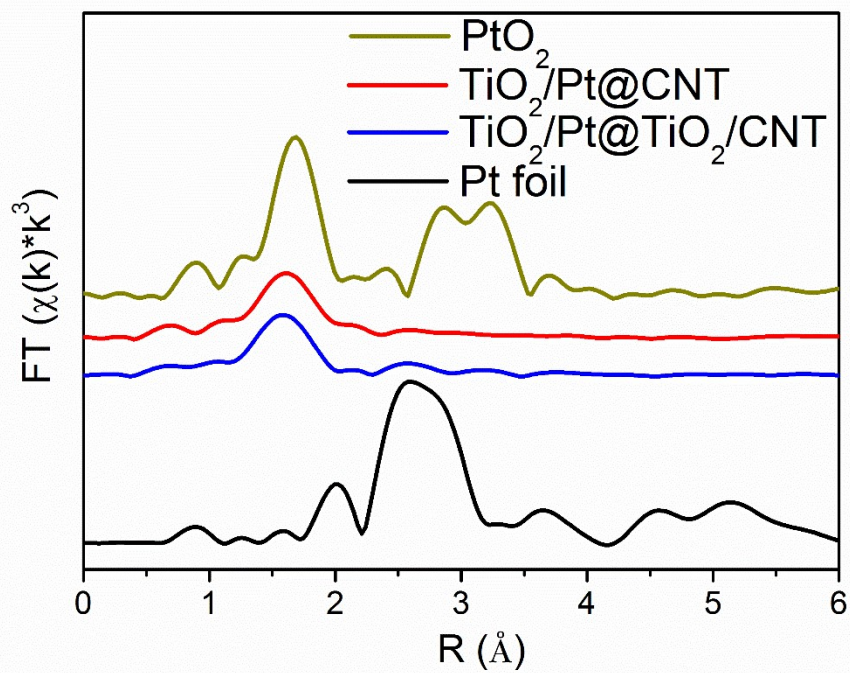


Figure S6. Pt L₃-edge Fourier transform k³-weighted EXAFS spectra of TiO₂/Pt@CNT, TiO₂/Pt@TiO₂/CNT and the reference samples.

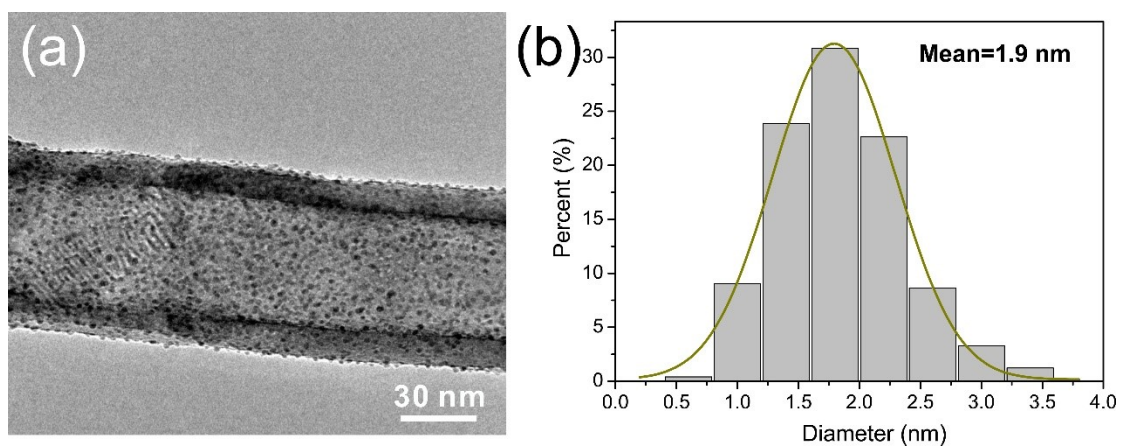


Figure S7. (a) TEM image of Pt/TiO₂ and (b) the corresponding particle size distribution of Pt nanoparticles in Pt/TiO₂.

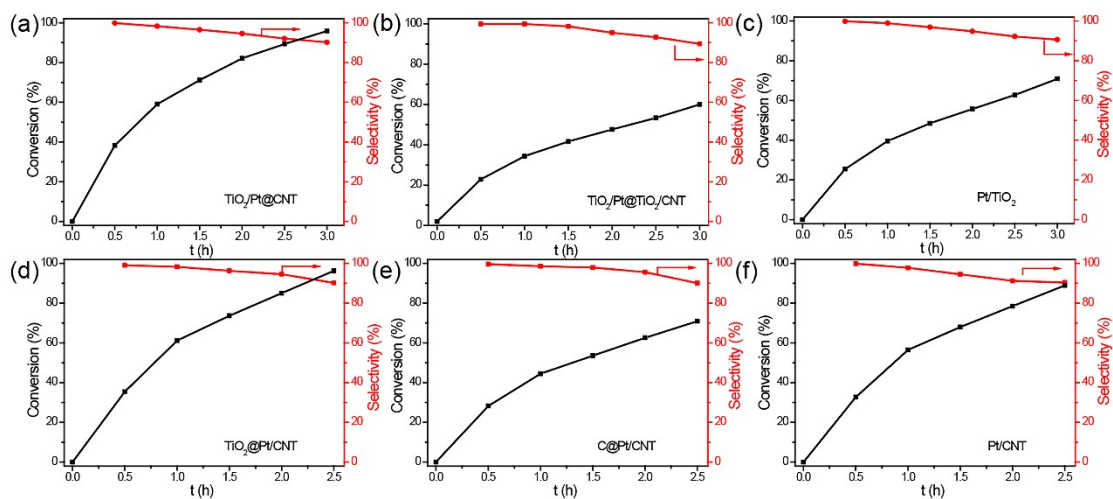


Figure S8. Variations of conversion and selectivity with reaction time in the oxidation of BA over (a) $\text{TiO}_2/\text{Pt}@\text{CNT}$, (b) $\text{TiO}_2/\text{Pt}@\text{TiO}_2/\text{CNT}$, (c) Pt/TiO_2 , (d) $\text{TiO}_2@\text{Pt}/\text{CNT}$, (e) $\text{C}@\text{Pt}/\text{CNT}$, and (f) Pt/CNT . Reaction conditions: 10 mL of H_2O , 4 mmol BA, 2.5 mL of H_2O_2 (30% in water), and catalysts at 90 °C. When these catalysts were used for BA oxidation, benzaldehyde was formed as the major product, and benzoic acid was produced as a byproduct.

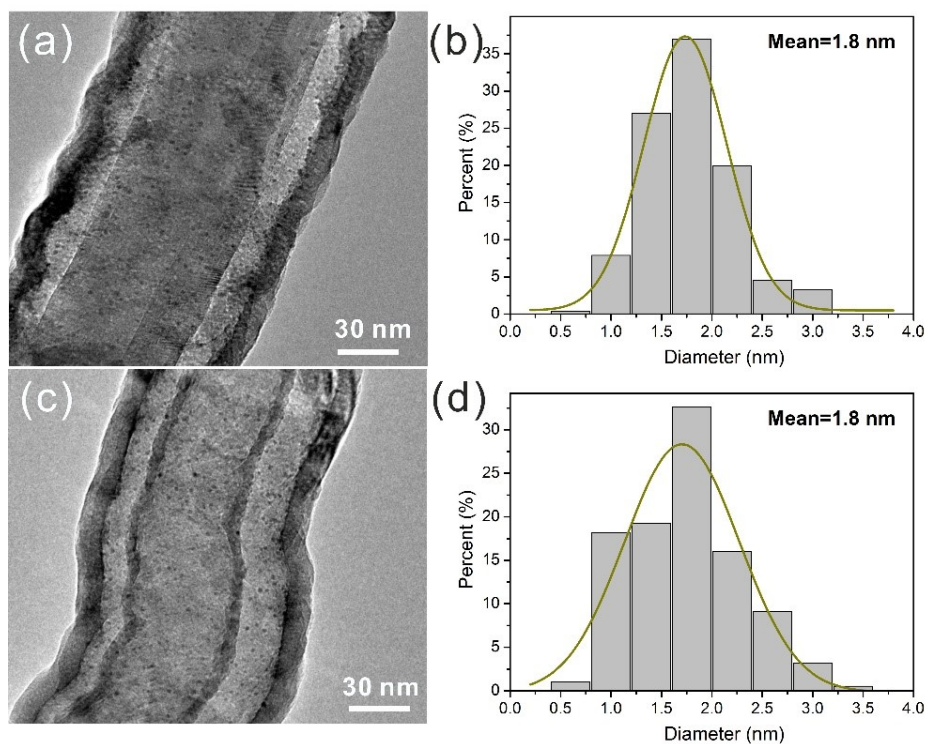


Figure S9. TEM images of (a) TiO₂/15Pt@CNT and (c) TiO₂/15Pt@TiO₂/CNT. The particle size distributions of Pt nanoparticles in (b) TiO₂/15Pt@CNT and (d) TiO₂/15Pt@TiO₂/CNT.

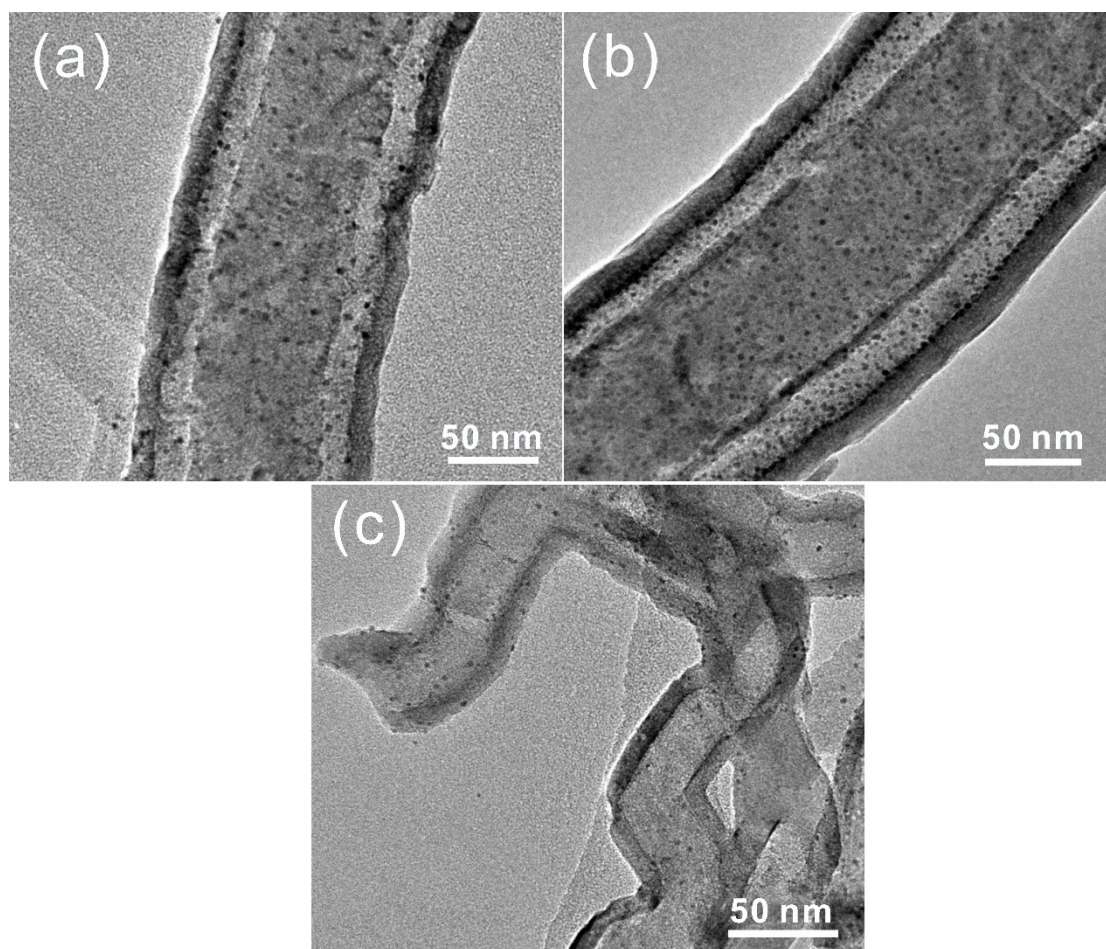


Figure S10. TEM images of (a) $\text{TiO}_2/\text{Pt}@/\text{CNT}$, (b) $\text{TiO}_2/\text{Pt}@/\text{TiO}_2/\text{CNT}$, and (c) Pt/TiO_2 after the fifth run. TEM images of the used $\text{TiO}_2/\text{Pt}@/\text{CNT}$ and $\text{TiO}_2/\text{Pt}@/\text{TiO}_2/\text{CNT}$ exhibit that the Pt nanoparticles are still confined in the outer TiO_2 nanotube. However, the vast majority of Pt nanoparticles of Pt/TiO_2 are detached after reused.

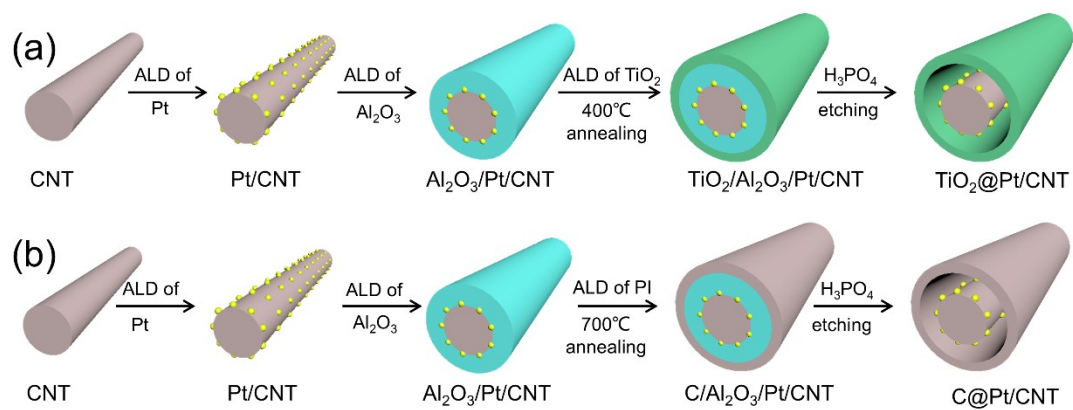


Figure S11. Synthetic illustrations of (a) TiO₂@Pt/CNT and (b) C@Pt/CNT catalysts.

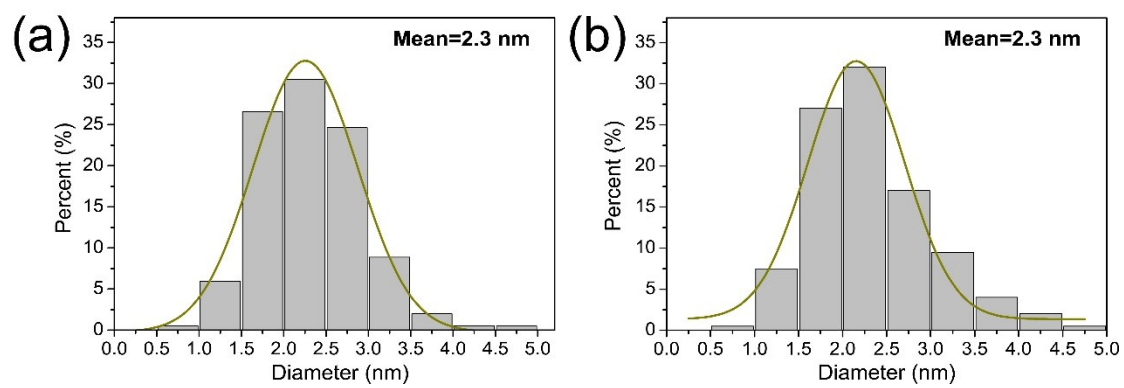


Figure S12. The particle size distributions of Pt nanoparticles in (a) $\text{TiO}_2@Pt/CNT$ and (b) $C@Pt/CNT$.

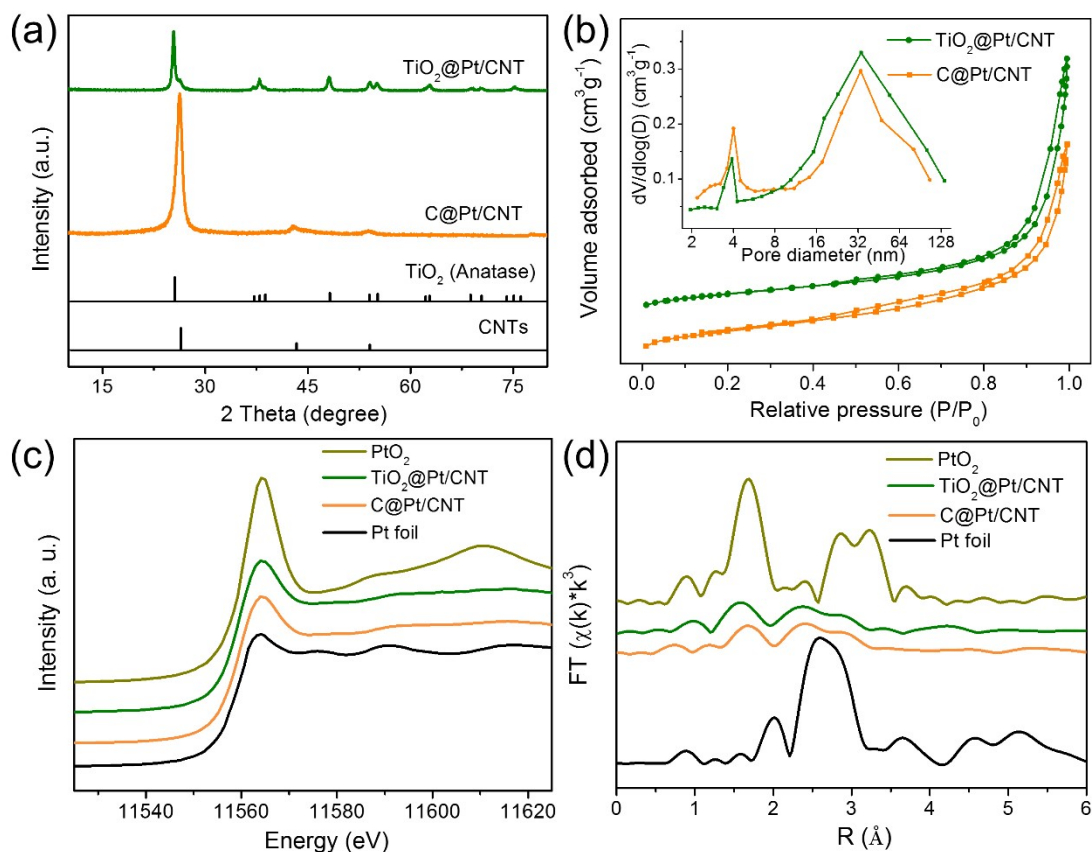


Figure S13. (a) XRD profiles, (b) N₂ adsorption-desorption isotherms, and (inset of b) pore size distribution plots of TiO₂@Pt/CNT and C@Pt/CNT. (c) Normalized intensity of Pt L₃-XANES and (d) the corresponding Fourier transform k³-weighted EXAFS spectra of TiO₂@Pt/CNT, C@Pt/CNT and the reference samples. For TiO₂@Pt/CNT, a strong diffraction peak at approximately 25.2° and several specific peaks are indexed to anatase TiO₂ (JCPDS No. 21-1272).² The weak diffraction peak at 26.2° is associated with CNTs. For C@Pt/CNT, a strong diffraction peak at 26.2° is associated with the graphite structure of CNTs.³ N₂ adsorption-desorption isotherms of the two catalysts exhibit type IV isotherms with H₃ hysteresis loops, suggesting the presence of mesoporous structure.⁴ The BET surface areas of TiO₂@Pt/CNTs and C@Pt/CNT are calculated to be 78.6, and 101.9 m² g⁻¹, respectively. The pore volumes of TiO₂@Pt/CNT and C@Pt/CNT are calculated to be 0.323 and 0.287 cm³ g⁻¹, respectively. The pore size distribution curves obtained by the BJH method show that the two catalysts have very similar pore size distributions. In the XANES spectra of the samples, the peak intensity of the white line for the as-prepared catalysts falls in the range between the Pt foil and PtO₂, suggesting that the Pt nanoparticles consist of both metallic Pt and PtO_x.⁵ No obvious differences between the spectra of TiO₂@Pt/CNT and C@Pt/CNT, indicating the electronic structure of Pt nanoparticles of the two catalysts are nearly identical. In their Fourier transforms of EXAFS data, Pt-Pt and Pt-O bond peaks were both observed, further verifying the coexistence of metallic Pt and PtO_x in Pt nanoparticles, which is consistent with the XANES analysis.

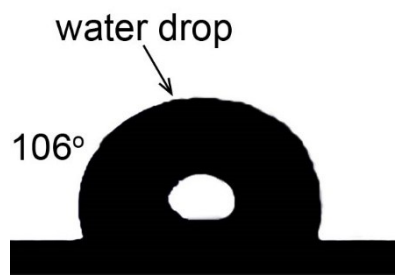


Figure S14. Static water droplet contact angle at the carbon nanofilms.

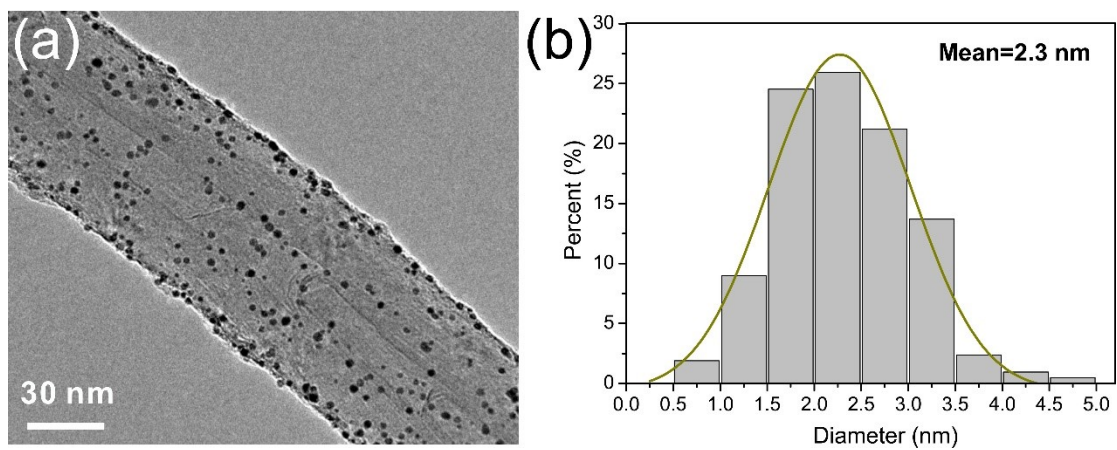


Figure S15. (a) TEM image of Pt/CNT and (b) the corresponding particle size distribution of Pt nanoparticles in Pt/CNT.

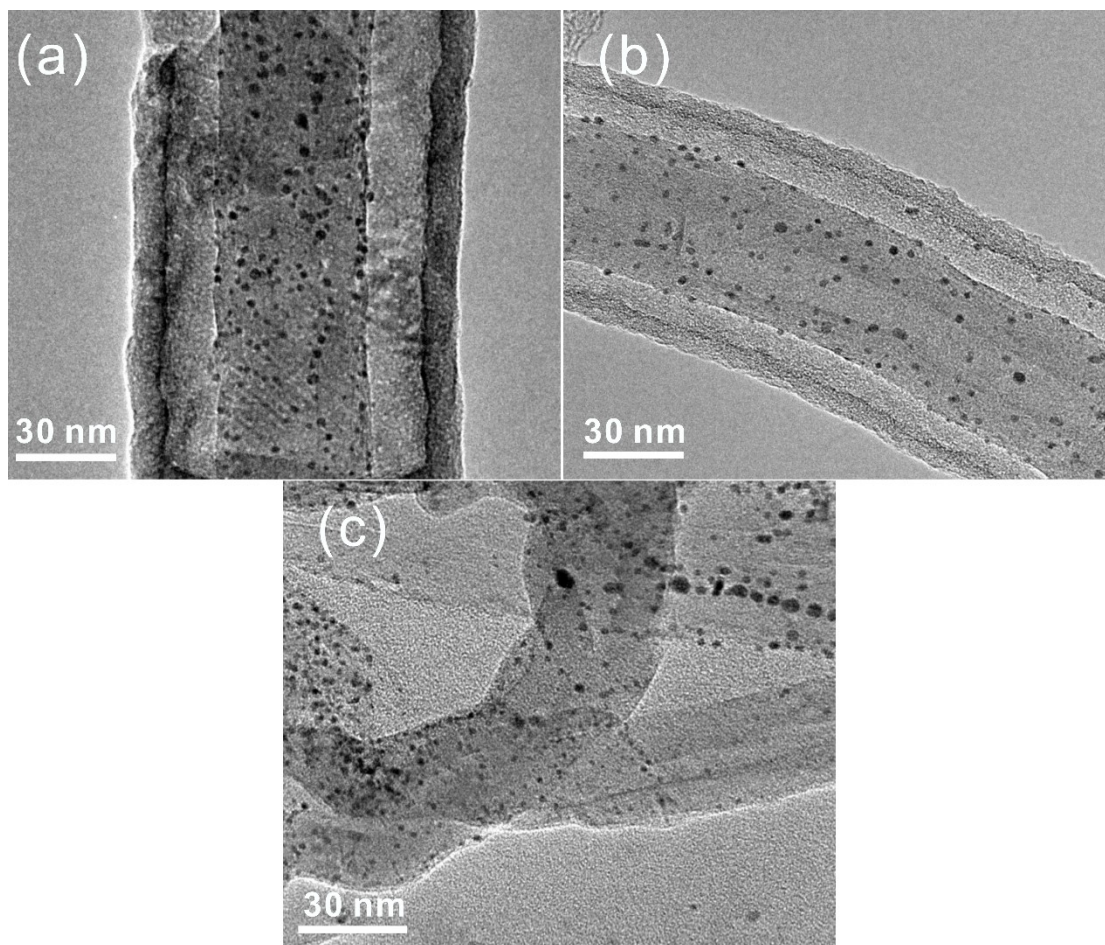


Figure S16. TEM images of (a) $\text{TiO}_2@\text{Pt}/\text{CNT}$, (b) $\text{C}@\text{Pt}/\text{CNT}$, and (c) Pt/CNT after the fifth run. TEM images of the used $\text{TiO}_2@\text{Pt}/\text{CNT}$ and $\text{C}@\text{Pt}/\text{CNT}$ exhibit that the Pt nanoparticles are relatively stable, while the vast majority of Pt nanoparticles of Pt/CNT are detached after reused.

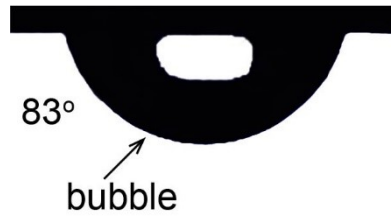


Figure S17. The gas-bubble contact angle under water for the carbon nanofilms.

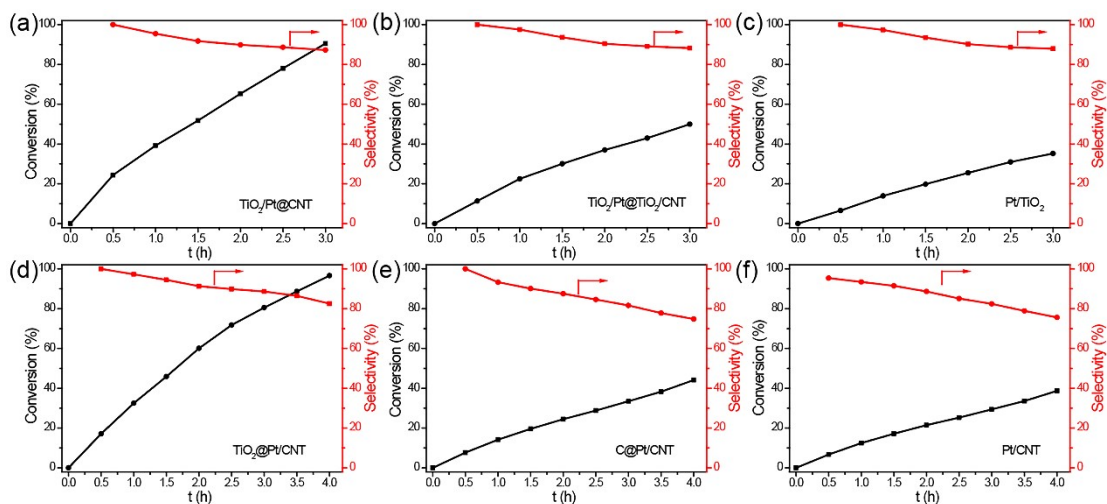


Figure S18. Variations of conversion and selectivity with reaction time in the hydrogenation of phenol over (a) $\text{TiO}_2/\text{Pt}@/\text{CNT}$, (b) $\text{TiO}_2/\text{Pt}@/\text{TiO}_2/\text{CNT}$, (c) Pt/TiO_2 , (d) $\text{TiO}_2@/\text{Pt}/\text{CNT}$, (e) $\text{C}@/\text{Pt}/\text{CNT}$, and (f) Pt/CNT . Reaction conditions: 20 mL of H_2O , 0.25 g phenol, and catalysts at 50 °C under H_2 atmosphere. When these catalysts were used for phenol hydrogenation, cyclohexanone was formed as the major product, and cyclohexanol was produced as a byproduct.

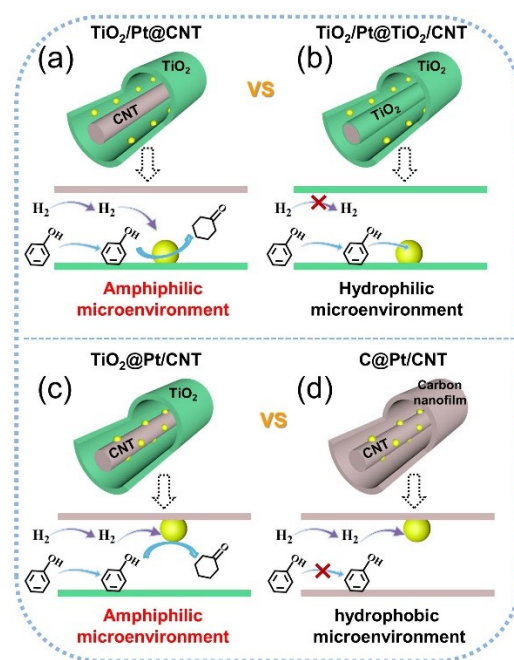


Figure S19. Schematic illustrations of the reactions occurring on (a) amphiphilic confined TiO₂/Pt@CNT, (b) hydrophilic confined TiO₂/Pt@TiO₂/CNT, (c) amphiphilic confined TiO₂@Pt/CNT, and (d) hydrophobic confined C@Pt/CNT catalysts. For each catalyst, the upper illustration is the semi-sectional view of the catalyst, and the lower illustration is the cross-sectional view of the nanochannel. The gray cylinders, green tubes, gray tubes and yellow balls represent CNTs, TiO₂ nanotubes, carbon nanofilms and Pt nanoparticles, respectively.

Table S1. Physicochemical characteristics of different catalysts.

Catalyst	S_{BET} ($\text{m}^2 \text{g}^{-1}$)	V_t ($\text{m}^3 \text{g}^{-1}$)	Pore size (nm)	Pt loading ^[a] (wt.%)	CO uptake ^[b] (mmol/g-Pt)
TiO ₂ /Pt@CNT	85.6	0.353	2.6; 3.9; 33.2	0.87	2.083
TiO ₂ /Pt@TiO ₂ /CNT	79.9	0.352	2.6; 3.9; 32.8	0.71	2.093
Pt/TiO ₂	71.3	0.399	2.5; 49.7	2.54	2.512
TiO ₂ @Pt/CNT	78.6	0.323	2.5; 3.8; 32.8	0.94	1.947
C@Pt/CNT	101.9	0.287	4.0; 33.4	1.65	1.963
Pt/CNT	71.0	0.176	3.9	1.84	2.002

[a] Measured by ICP-AES.

[b] The CO uptake was tested by CO-pulse adsorption measurement.

Table S2. Catalytic data for the oxidation of BA over the Pt-based catalysts with and without H₃PO₄ etching.

Entry	Catalyst	Solvent	Conversion ^[b] (%)
1	---	H ₂ O	2.36
2	Pt/TiO ₂	H ₂ O	51.3
3	Pt/TiO ₂ -H ₃ PO ₄ ^[a]	H ₂ O	50.5
4	Pt/CNT	H ₂ O	53.3
5	Pt/CNT-H ₃ PO ₄ ^[a]	H ₂ O	50.9

[a] Pt/TiO₂ and Pt/CNT catalysts were further treated with 10 wt.% H₃PO₄ solution, getting Pt/TiO₂-H₃PO₄ and Pt/CNT-H₃PO₄, respectively.

[b] Reaction conditions: 10 mL of H₂O, 4 mmol BA, 2.5 mL of H₂O₂ (30% in water), and 20 mg catalysts at 90 °C for 1 h.

Table S3. Catalytic data for the oxidation of BA over the different catalysts.

Entry	Catalyst	Solvent	TOF (h ⁻¹) ^[c]
1	TiO ₂ /Pt@CNT ^[a]	H ₂ O	3774.4
2	TiO ₂ /Pt@TiO ₂ /CNT ^[a]	H ₂ O	2080.4
3	TiO ₂ /Pt@CNT ^[b]	Toluene	438.5
4	TiO ₂ /Pt@TiO ₂ /CNT ^[b]	Toluene	344.3

[a] Reaction conditions: 10 mL of H₂O, 4 mmol BA, 2.5 mL of H₂O₂ (30% in water), and catalysts at 90 °C.

[b] Reaction conditions: 10 mL of toluene, 1 mmol BA, 625 μL of H₂O₂ (30% in water), and catalysts at 90 °C.

[c] The number of BA molecules converted per atom of exposed Pt on the surface per unit time at initial times of 30 min.

Table S4. Physicochemical characteristics of TiO₂/15Pt@CNT and TiO₂/15Pt@TiO₂/CNT.

Entry	Catalyst ^[a]	Solvent	Pt loading ^[b] (wt.%)	CO uptake (mmol/g-Pt)	TOF ^[c] (h ⁻¹)
1	TiO ₂ /15Pt@CNT	H ₂ O	0.40	2.733	3855.4
2	TiO ₂ /15Pt@TiO ₂ /CNT	H ₂ O	0.33	2.781	2373.3

[a] Reaction conditions: 10 mL of H₂O, 4 mmol BA, 2.5 mL of H₂O₂ (30% in water), and catalysts at 90 °C.

[b] Measured by ICP-AES.

[c] The TOF values were calculated at the initial 30 min.

Table S5. Catalytic data for the oxidation of BA over the conventional catalysts.

Entry	Catalyst	Solvent	TOF ^[a] (h ⁻¹)
1	Pt/TiO ₂	H ₂ O	2084.1
2	Pt/CNT	H ₂ O	3344.6

[a] Reaction conditions: 10 mL of H₂O, 4 mmol BA, 2.5 mL of H₂O₂ (30% in water), and catalysts at 90 °C, the TOF values were calculated at the initial 30 min.

Table S6. Catalytic data for the oxidation of BA over the different stirring rates.

Entry	Catalyst	Stirring rate (rpm)	TOF ^[a] (h ⁻¹)
1	TiO ₂ /Pt@CNT	900	3774.4
2	TiO ₂ /Pt@TiO ₂ /CNT	900	2080.4
3	TiO ₂ /Pt@CNT	1200	3891.6
4	TiO ₂ /Pt@TiO ₂ /CNT	1200	2137.3

[a] Reaction conditions: 10 mL of H₂O, 4 mmol BA, 2.5 mL of H₂O₂ (30% in water), and catalysts at 90 °C, the TOF values were calculated at the initial 30 min.

Table S7. Catalytic data for the oxidation of BA over amphiphilic confined catalysts with different thicknesses of sacrificial Al₂O₃.^[a]

Entry	Catalysts	Conversion (%)	TOF ^[c] (h ⁻¹)
1	TiO ₂ /Pt@CNT-0	8.6	--- ^[d]
2	TiO ₂ /Pt@CNT-8	44.0	4335.0
3	TiO ₂ /Pt@CNT-16	38.3	3774.4
4	TiO ₂ /Pt@CNT-32	21.1	2079.4
5	TiO ₂ /Pt@CNT-64 ^[b]	23.0	2270.4

[a] The amphiphilic confined catalysts with different thicknesses of sacrificial Al₂O₃ were denoted as TiO₂/Pt@CNT-x, where x refers to the confined space size, x=0, 8, 16, 32, and 64 nm.

[b] Due to the large confined space size of TiO₂/Pt@CNT-64, the thickness of the outer TiO₂ nanotubes is increased to ensure the structural stability of the catalyst. The cycle numbers of ALD Al₂O₃ and TiO₂ are 480 and 600, respectively.

[c] Reaction conditions: 10 mL of H₂O, 4 mmol BA, 2.5 mL of H₂O₂ (30% in water), and catalysts at 90 °C for 30 min. the TOF values were calculated at the initial 30 min.

[d] The TOF value of TiO₂/Pt@CNT-0 is not calculated because the Pt nanoparticles are covered by TiO₂ layer.

When the distance between the TiO₂ nanotube and CNT is 0 nm, TiO₂/Pt@CNT-0 exhibits a low catalytic performance due to the little exposed Pt atoms. The TOF value of TiO₂/Pt@CNT-8 is the highest among these catalysts. When it comes to a larger distance (32 or 64 nm), the catalytic performance of TiO₂/Pt@CNT-32 and TiO₂/Pt@CNT-64 decreases sharply. And the TOF values of the catalysts don't significantly change when the distance increases from 16 to 32 nm. At this point, the distance between these surfaces is so large that their cooperative chemistry cannot be observed.

Table S8. Catalytic data for the oxidation of BA over the different catalysts.

Entry	Catalyst	Solvent	TOF (h ⁻¹) ^[c]
1	TiO ₂ @Pt/CNT ^[a]	H ₂ O	3726.5
2	C@Pt/CNT ^[a]	H ₂ O	2950.4
3	TiO ₂ @Pt/CNT ^[b]	Toluene	397.4
4	C@Pt/CNT ^[b]	Toluene	201.4

[a] Reaction conditions: 10 mL of H₂O, 4 mmol BA, 2.5 mL of H₂O₂ (30% in water), and catalysts at 90 °C.

[b] Reaction conditions: 10 mL of toluene, 1 mmol BA, 625 μL of H₂O₂ (30% in water), and catalysts at 90 °C.

[c] The TOF values were calculated at the initial 30 min.

Table S9. Catalytic data for phenol hydrogenation over the various catalysts.

Entry	Catalyst	Solvent	TOF ^[a] (h ⁻¹)
1	TiO ₂ /Pt@CNT	H ₂ O	3193.0
2	TiO ₂ /Pt@TiO ₂ /CNT	H ₂ O	1484.5
3	Pt/TiO ₂	H ₂ O	727.0
4	TiO ₂ @Pt/CNT	H ₂ O	2383.6
5	C@Pt/CNT	H ₂ O	1061.2
6	Pt/CNT	H ₂ O	912.2

[a] Reaction conditions: 20 mL of H₂O, 0.25 g phenol, and catalysts at 50 °C under H₂ atmosphere. The number of phenol molecules converted per atom of exposed Pt on the surface per unit time at initial times of 30 min.

Reference

- 1 Z. Lu, W. Xu, J. Ma, Y. Li, X. Sun and L. Jiang, *Adv. Mater.*, 2016, **28**, 7155-7161.
- 2 X. Zhou, V. Haublein, N. Liu, N. T. Nguyen, E.M. Zolnhofer, H. Tsuchiya, M.S. Killian, K. Meyer, L. Frey and P. Schmuki, *Angew. Chem. Int. Ed.*, 2016, **55**, 3763-3767.
- 3 J. Zhang, C. Chen, W. Yan, F. Duan, B. Zhang, Z. Gao and Y. Qin, *Catal. Sci. Technol.*, 2016, **6**, 2112-2119.
- 4 D. Liu, G. Li, J. X. Liu, Y. H. Yi, *Fuel*, 2019, **244**, 196-206.
- 5 J. K. Zhang, W. Y. Chen, H.B. Ge, C. Q. Chen, W. J. Yan, Z. Gao, J. Gan, B. Y. Zhang, X. Z. Duan and Y. Qin, *Appl. Catal. B: Environ.*, 2018, **235**, 256-263.